crystals

MDPI

Article

Stress-Based Model for Calculating the Opening Angle of Notch Cracks in a Magnesium Alloy under Multiaxial Fatigue

Henrique Videira [1], Vitor Anes [1,2,*] and Luis Reis [1,*]

[1] Mechanical Engineering Institute (IDMEC), Instituto Superior Técnico, Universidade de Lisboa, 1, 1049-001 Lisboa, Portugal; henrique.videira@tecnico.ulisboa.pt
[2] Mechanical Engineering Department, Instituto Superior de Engenharia de Lisboa, Instituto Politécnico de Lisboa, 1, 1959-007 Lisboa, Portugal
* Correspondence: vitor.anes@isel.pt (V.A.); luis.g.reis@tecnico.ulisboa.pt (L.R.)

Abstract: This paper presents a model to calculate the opening angle of crack initiation in notched fractures subjected to multiaxial loading. To validate the proposed model, a study was performed on polished AZ31B-F magnesium alloy specimens under multiaxial high-cycle fatigue loading. The specimens exhibited a notch in the smaller cross-sectional area, which was created with a special drilling jig to promote the formation of fatigue cracks in this localized area of the specimen. The load paths used in the experiments and numerical analyses were proportional and non-proportional, resulting in different stress states in the crack front opening, which were determined by finite element analysis to validate the proposed model. To obtain more accurate numerical results for these estimates, these finite element analyses were performed using the nonlinear Chaboche plasticity model of ABAQUS® 2021 software. A sensitivity analysis was also performed to determine which load component—axial or torsional—has a greater influence on the fatigue strength and contributes significantly to the crack opening process. The results show that the type of load path and the stress level of each load component—axial and torsional—has a strong influence on the opening angle of the notch crack and the fatigue lifetime of the specimen. This result is confirmed not only by the experimentally determined fatigue strength, but also by a fractographic analysis performed on the surface of the specimens for both load paths. Moreover, the results show an acceptable correlation between the experimental results and the estimates obtained with the proposed model and the stresses obtained with the finite element analysis.

Keywords: multiaxial fatigue; notch crack opening angle; AZ31B-F magnesium alloy; stress-based model

Citation: Videira, H.; Anes, V.; Reis, L. Stress-Based Model for Calculating the Opening Angle of Notch Cracks in a Magnesium Alloy under Multiaxial Fatigue. *Crystals* **2024**, *14*, 211. https://doi.org/10.3390/cryst14030211

Academic Editors: Cuiyun Liu, Ruixiao Zheng and Umberto Prisco

Received: 19 January 2024
Revised: 10 February 2024
Accepted: 19 February 2024
Published: 23 February 2024

1. Introduction

Structural failure is often caused by fatigue cracks, which frequently develop and propagate in critical areas, usually due to complex geometric shapes and/or multiaxial loading conditions.

In this context, the development of fatigue cracks and the orientation or propagation of crack growth are receiving increasing attention in research, as they are crucial for an accurate assessment of fatigue crack life and for analyzing the ultimate failure modes of cracked components and structures [1–3].

In practice, components and structures not only exhibit geometric features that lead to local stress/strain concentrations, but they are also subjected to multi-axial load histories with different amplitudes in operation, leading to a complex combination of factors that is not yet fully understood. This explains why, since the beginning of the 20th century, enormous efforts have been made worldwide to develop robust design methods that are suitable for solving such a difficult problem [4].

A look at the state of the art shows that the international scientific community has focused heavily on the formulation of fatigue parameters whose definition is based on

either nominal linear elastic–plastic cyclic stresses or nominal elasto-plastic cyclic strains [5]. For notched components operating in the high cyclic fatigue range, various multiaxial fatigue criteria were developed in the 1940s and 1950s based on the pioneering work of Neuber [6] and Peterson [7]. These approaches model the adverse effects of stress risers by performing the stress analysis in terms of nominal values [8–11], but also by directly post-processing the local linear elastic stress/strain fields in the vicinity of the geometric features under investigation [4,12,13]. Nevertheless, there is little work addressing the fatigue strength of notched components, especially for new materials such as magnesium alloys. Therefore, further work in this area is required to fully understand the fatigue phenomena of notched components, especially those made of magnesium alloys subjected to multiaxial loads.

Magnesium is a very common metal. It makes up around two percent of the earth's crust and is the third most common element dissolved in seawater [14], which contains about 0.13% magnesium, or about 1.1 kg per cubic meter [15].

Magnesium belongs to the family of alkaline earth metals [16], and its alloys belong to the light metals [17] and have enormous potential for mechanical and structural applications [18], mainly because they are the lightest construction material, i.e., they have high specific strength and low density [16], interesting damping properties [19], good machinability and recyclability. They also contribute to environmental protection [14], as they promote fuel efficiency by reducing the weight of means of transportation [15], which in turn, counteracts climate change. Magnesium is mainly used as a casting and wrought alloy. Due to its close packed hexagonal crystal structure (HC), magnesium is difficult to form by cold rolling and is therefore mainly a cast material. Magnesium alloys are easy to forge or extrude and are characterized by good fatigue strength, although the notched bar impact strength is rather low [16]. In wrought magnesium alloys, cracking is also associated with material inclusions, but in most cases, twin deformations and slip bands associated with twin density flow are the main cause of cracking. Crack propagation generally occurs along the fields of the deformation twins [20–22].

All these properties have attracted the attention of the automotive and aerospace industries. In the aerospace industry, magnesium alloys have so far been used for non-structural applications [23,24], but there is a growing interest in extending the use of magnesium alloys to structural components as the corrosion resistance of these alloys has recently improved. Magnesium alloys are also used in the military sector, particularly in helicopters and drones [23].

Despite the advantages attributed to magnesium alloys, they exhibit non-standard mechanical behavior, which poses an additional challenge in evaluating their mechanical resistance when subjected to cyclic and multi-axial loads with variable amplitude. This has particular implications for the design of magnesium alloy structures and components. The peculiarity of their mechanical behavior results from their compact hexagonal crystal structure, which influences the way in which the slip planes of the crystal structure occur. In particular, the occurrence of the phenomenon of twinning and de-twinning under cyclic loading leads to eccentric and asymmetric hysteresis cycles. As a result, this behavior leads to different cyclic yield stresses in tension and compression according to the cyclic development and adaptation of the hysteresis loops, which typically exhibit a hardening in tension and a slight softening in compression.

It is interesting to note that the cyclic yield stress of magnesium can increase cyclically and can be higher than the monotonic yield stress, which is due to the cyclic hardening process. Therefore, the yield stress determined in uniaxial tensile tests cannot be used to estimate the mechanical resistance of magnesium alloys under cyclic loading. This limitation becomes even more important when magnesium alloys are subjected to multiaxial loads leading to multiaxial cyclic hardening/softening, which increases the complexity of the problem. Furthermore, it has been shown that the uniaxial fatigue limit approach (uniaxial normal and shear loading), traditionally used in multiaxial fatigue models to estimate fatigue strength, is very unsuitable for estimating the fatigue life of magnesium alloys [25].

In this sense, and due to the increasing complexity of the cyclic behavior of magnesium alloys, the development of new strategies to capture their mechanical behavior has been promoted, resulting in more complex methods than the traditional ones being applied to capture the cyclic mechanical behavior, leading to the so-called phenomenological models, also known as empirical models, which relay on test data capture the evolution of a damage parameter or mechanical properties [26]. In fact, it is very difficult or even impossible to model/estimate this cyclic behavior without resorting to phenomenological models, i.e., models that represent the cyclic behavior of these materials, which is usually determined by experimental data and fitting methods [27]. This is so true that current finite element simulation software is not prepared to model the cyclic behavior of these materials. Therefore, alternative strategies such as those used in this article are necessary, where the cyclic behavior of the material is modeled based on experiments, and strategies such as the use of external software (e.g., Matlab version R2022) are employed to update the mechanical properties of the material throughout the testing period during FEA simulations [28]. In these situations, phenomenological models make an important contribution to solving the problem of estimating the mechanical behavior of materials whose mechanical behavior is not standardized. It would indeed be advantageous to have a universal model that could estimate the mechanical response to all materials based just on the stress or strain tensor and one or another easily accessible property of the material, but this is not the reality, especially not for magnesium alloys.

The aim of this paper is to present a stress-based model that can be used to calculate the opening angle of the notch crack of a magnesium alloy under biaxial fatigue in a high-cycle fatigue loading regime. Furthermore, the fracture angle under different load path conditions is discussed. The presence of notches has a significant impact on shortening the lifetime of components [29], and for magnesium alloys, the number of studies available in the literature on this area is very limited. With this in mind, this paper aims to investigate the effects of different multiaxial loading paths with different loading characteristics on notched specimens tested in the laboratory for fatigue crack growth and fatigue strength. The results obtained contribute directly to the knowledge of fracture mechanics and maintenance activities of magnesium alloy components and structures.

2. Materials and Methods

2.1. Material, Specimen Shape and Test Method

The material investigated in this study is a commercially available extruded AZ31B-F magnesium alloy. To characterize the mechanical properties of this material, test procedures were performed according to the standard methods described in ASTM E8 [30], and ASTM E606/E606M-21 [31]. The chemical composition of AZ31BF is listed in Table 1, and the technical sketch showing the geometry, dimensions and notch of the sample is shown in Figure 1. The cyclic properties of AZ31BF magnesium alloy were determined by analyzing the experimental data, namely the elastic, plastic, monotonic and cyclic properties, listed in Table 2.

Table 1. Chemical composition of the magnesium alloy AZ31B-F.

Chemical Composition (in wt%)								
				AZ31B				
Mg	Al	Zn	Mn	Fe	Ni	Cu	Ca	Si
Balance	3.1	1.05	0.54	0.0035	0.0007	0.0008	0.04	0.1

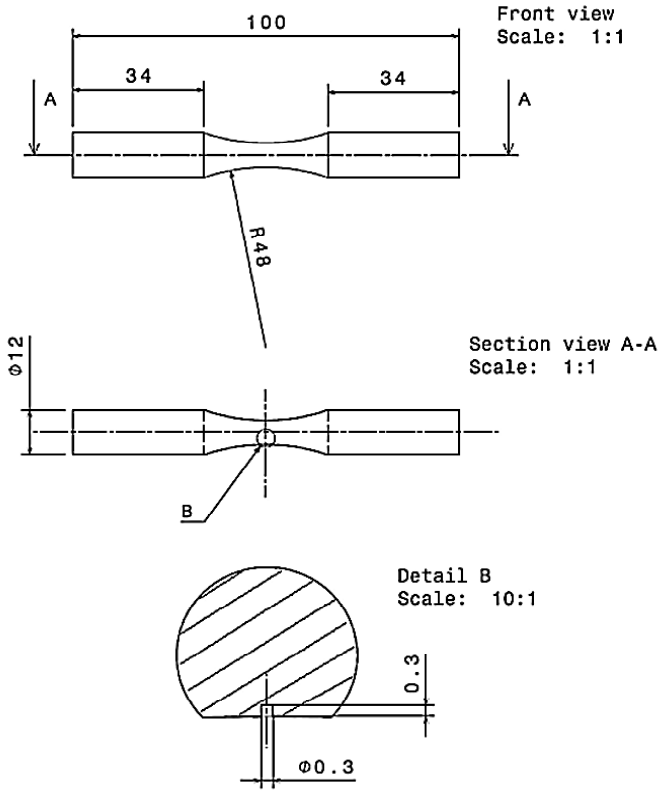

Figure 1. Technical sketch of the specimen.

Table 2. Elastic, plastic, monotonic and cyclic properties of the magnesium alloy AZ31B-F.

Elastic Properties	
Young's Modulus [GPa]	44
Modulus of shear [GPa]	15
Coefficient of Poisson	0.35
Plastic Properties	
True Stress [MPa]	**True Strain [%]**
212	0.0
183	0.5
241	0.7
256	0.9
256	1.2
Monotonic and cyclic properties	
Tensile strength [R_m (MPa)]	290
Monotonic yield strength [R_p (MPa)]	211
Cyclic yield strength [R'_p (MPa)]	95
Elongation at failure [A (%)]	14
Cyclic strength coefficient [K' (MPa)]	576
Hardening exponent [n']	0.17
Fatigue strength coefficient [σ'_f (MPa)]	450
Fatigue strength exponent [b]	−0.12
Fatigue ductility coefficient [ε_f]	0.26
Fatigue ductility exponent [c]	−0.71

Fatigue tests were carried out in a servo-hydraulic machine, Instron model 8800, with a stress ratio of R = −1, at a frequency of 2 Hz and a room temperature of 20 °C. Two biaxial cyclic loading paths were chosen for this study, see Figure 2. The first is an in-phase, proportional loading path (PP) Figure 2a), and the second is a non-proportional, 90° out-of-

phase loading path (OP), Figure 2b). All tests were performed at room temperature and ended when the samples were completely separated.

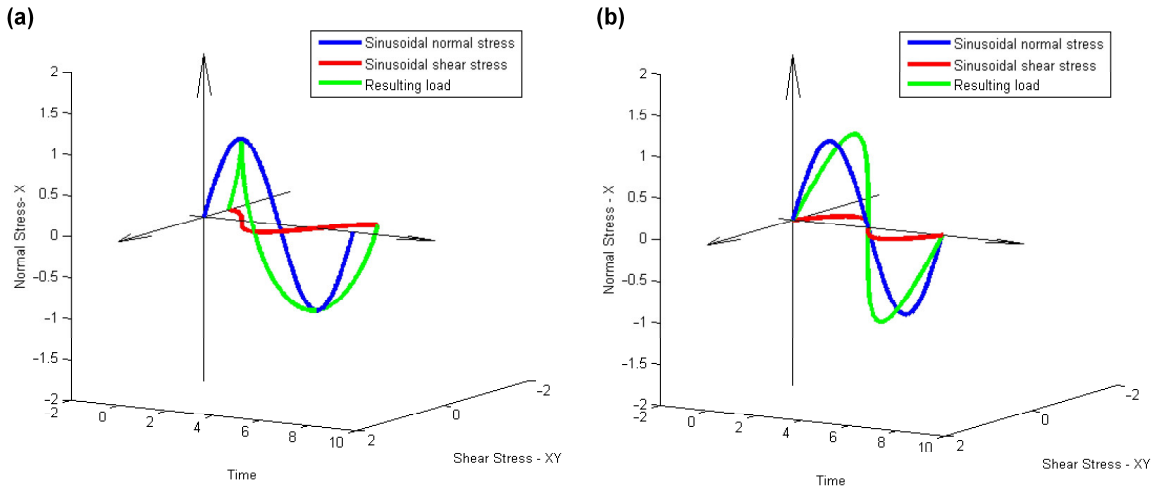

Figure 2. 3D loading Path: (**a**) non proportional; and (**b**) proportional.

Figure 2 shows the stress–time curve for normal and shear stress amplitudes, with the blue line representing the sinusoidal normal stress, the red line the sinusoidal shear stress and the green line the load path as a result of the combination of normal and shear stresses. Table 3 shows the stress amplitudes considered in fatigue tests for normal and shear stresses.

Table 3. Stress amplitudes and stress ratios used in fatigue tests.

Sigma [Mpa]	Tau [Mpa]	Stress Ratio	von Mises
54	31	0.577	77
60	35	0.577	85
67	39	0.577	95
71	41	0.577	100
74	43	0.577	105
78	45	0.577	110

2.2. Characterization of the Cyclic Behavior of the AZ31BF

Structural metals react differently to cyclic and monotonic stresses. This depends on various factors, from the type of microstructure to heat treatments and the type of load path. One example of this is the difference between the monotonic and cyclic yield stress that occurs during cyclic hardening. Magnesium alloys tend to exhibit a more pronounced cyclic hardening behavior on the tensile side of the cyclic load; on the compressive side, this hardening is almost negligible. Hardening occurs when the cyclic condition influences the plasticity of the material in such a way that the cyclic yield stress is higher than the monotonic yield stress and the cyclic curve is higher than the monotonic curve [32].

This is mainly due to grain dislocations of the material as a result of cyclic load, purity, inherent lattice behavior such as twinning or casting transformation processes [33–37]. It can be concluded that fatigue models used to estimate crack initiation areas and fatigue life must take into account the cyclic behavior of the material [37–39]. In wrought magnesium alloys, fatigue cracking processes are also associated with material inclusions, but in most cases, the deformation of the twin and the slip bands associated with the twin density flow are the main cause of cracking.

The cyclic material curve can be used as a reference for fatigue loading to perform elastic–plastic numerical simulations. However, the process of fatigue crack initiation leads to micro-notches, which in turn, cause stress raisers that are very likely to lead to local

plasticity [32]. Furthermore, the occurrence of fatigue cracks is associated with plasticity, which leads to the conclusion that the effects of plasticity on the stress and strain states must not be neglected when determining the crack initiation plane [21,40,41].

For this study, the elastic–plastic behavior of the material is based on the tests with bulk material and is therefore used as an approximation for the evaluation of local plasticity [32]. The curves shown in Figure 3 were determined on the basis of the ASTM E8 and ASTM 606 standards. The cyclic response of the AZ31B-F alloy at different strain hysteresis loops shows different yield stresses in tension and compression. The compressive yield stress is close to the monotonic value, while the tensile stress is about 26% higher than the monotonic yield stress (203 MPa and 256 MPa, respectively) [32].

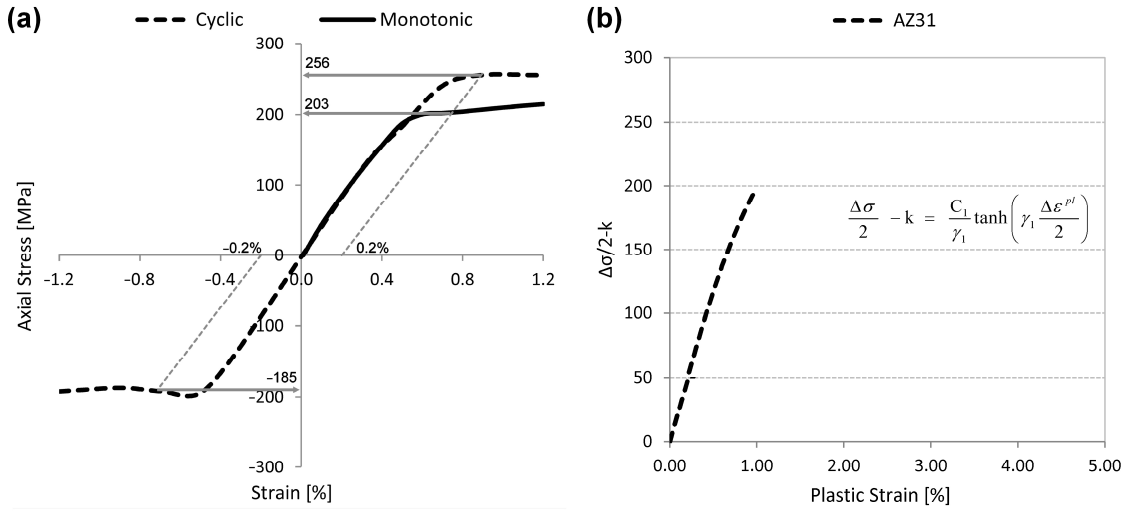

Figure 3. AZ31B-F: (**a**) Magnesium alloy monotonic and cyclic behavior, (**b**) calibration test of the Chaboche plasticity model.

2.3. Chaboche Plasticity Model

In general, plasticity models have three main components to capture a material's response to plastic deformation. One of these components is the yield function, which determines when a material yields. The most common yield criterion is the von Mises function, where a combination of principal stresses on the octahedral plane determines the yield point. The second part of plasticity models is the yield rule, which is based on constitutive equations, in which the stresses and strains are calculated using the incremental plasticity method, in which the next plastic deformation depends on the previous one. This rule is generally based on the Drucker postulate [42], where the increments of plastic strain are perpendicular to the yield surface defined by the yield function. The third part is the strain hardening rule, which defines the changes on the yield surface during plastic deformation [43]. The Chaboche plasticity model is a non-linear kinematic hardening model. The yield function F is given through the follow equation:

$$F = \sqrt{\frac{3}{2}(S-\alpha):(S-\alpha)} - K = 0 \quad (1)$$

where S is the deviatoric stress, α is the back stress, and K is the yield stress [44,45]. The kinematic hardening is determined by the back stress tensor; this contribution of the model component is related to the translation of the yield surface [32]. The calculations of the back stress tensor are contained in the following equations:

$$\{\alpha\} = \sum_{i=1}^{n} \{\alpha_i\} \quad (2)$$

$$\{\Delta\alpha\}_j = \frac{2}{3}C_1\left\{\Delta\varepsilon^{pl}\right\} - \gamma_i\{\alpha_i\}\Delta\hat{\varepsilon}^{pl} + \frac{1}{C_i}\frac{dC_i}{d\theta}\Delta\theta\{\alpha\} \quad (3)$$

where $\Delta\varepsilon^{pl}$ is the accumulated plastic strain, θ is temperature, and C_1 and γ_1 are the Chaboche material parameters. In Equation (3), the strain hardening modulus and back stress variation (recall term) are represented by the first and second terms, respectively. The third term refers to the temperature change. According to the ABAQUS® 2021 Reference Manual, see [46], the Chaboche plasticity model allows for the use of different kinematic models and material constants. Here, C_1 and γ_1 are model inputs for the kinematic model. In this study, C_1 and γ_1 are determined based on the cyclic material response presented in the previous subsection.

2.4. Chaboche Model Calibration

The material parameters of the Chaboche plasticity model can be determined by stress–strain tests under stabilized hysteresis loops. Using the values of plastic strain and the inherent recall term, which is the difference between the applied stress amplitude $\Delta\sigma/2$ and the cyclic yield stress (K) of the material at a fixed total strain, the relationship between these two values can be fitted using Equation (4). The material constants C_1 and γ_1 can be determined by a fitting procedure.

$$\frac{\Delta\sigma}{2} - K = \frac{C_1}{\gamma_1}tanh\left(\gamma_1\frac{\Delta\varepsilon^{pl}}{2}\right) \quad (4)$$

Table 4 shows the input parameters used in the ABAQUS® finite element analysis.

Table 4. Chaboche input parameters used in the numerical simulation for the material.

Material	C_1	γ_1
AZ31B	25,000	90

3. Theoretical Analysis and Model Proposal

3.1. Stress Plane Approach

Since fatigue cracking occurs under high-cycle fatigue loading for a particular material at the surface, a stress plane approach was considered in the current study to support model considerations and development. These conditions are based on the following generic stress tensor:

$$\overline{\sigma} = \begin{bmatrix} \sigma_{xx} & -\tau_{xy} & 0 \\ -\tau_{xy} & \sigma_{yy} & 0 \\ 0 & 0 & 1 \end{bmatrix} \quad (5)$$

where the term σ_{xx} is the stress in the direction xx, and the term σ_{yy} is the stress in the direction yy. The term τ_{xy} is the shear stress in the xy direction of the specimen. The loading paths assumed in the experiments are the proportional (PP) and non-proportional (OP), i.e., a combination of normal and torsion loads applied simultaneously with different phase angles between each load, as previously described in Figure 2. In this case, the general normal stress due to the axial load is given by the following analytical expression:

$$\sigma = \frac{F}{\pi R^2} \quad (6)$$

where F is the term for the normal load, and R is the term for the radius of the sample throat. In this case, the general shear stress due to the torsional load is given by the following analytical expression:

$$\tau = \frac{TR}{J} \quad (7)$$

where T is the term for the torsion, R is the term for the radius of the specimen throat, and J is the polar moment of inertia. In this case, the polar moment of inertia for a generic cylindrical body is given by the following analytical expression:

$$J = \frac{\pi R^4}{2} \tag{8}$$

Finally, if Equation (8) is substituted into Equation (7), the final analytical expression for the shear stress due to torsion is obtained by the following analytical expression:

$$\tau = \frac{2T}{\pi R^3} \tag{9}$$

3.2. Proposed Approach

Physically, the proposed model uses the angle between the components of the shear stress in xy direction, and the respective normal stresses in x and y. It is assumed that the combination of these two stresses persists in a particular plane, a plane that is more stressed than the others, where crack initiation and propagation are expected to occur.

Since the proposed model is based on stresses and these stresses may change over time due to hardening/softening, the proposed model requires that the developed stresses be determined by FEA simulations. The obtained stresses are then used in the proposed model to estimate the crack opening angle.

The estimated orientation of the crack initiation plane is then adjusted using the beta parameters determined by the experiments described in this paper. With these parameters, it is possible to tune the model expression to the cyclic behavior of the magnesium alloy in question. In practice, it is possible to estimate the crack initiation plane for magnesium alloys by inserting the beta values from Table 5 of the manuscript into expression 10, depending on the type of loading (proportional (PP) or non-proportional (OP)).

$$\begin{aligned}\theta^{NCOA} = &\left\{\left(\text{atan}\left(\frac{S_{22}}{S_{23}}\right) - \text{atan}\left(\frac{S_{22}}{S_{23}}\right) * \beta_{max}^{Axial}\right) - \left(\text{atan}\left(\frac{S_{23}}{S_{33}}\right) - \text{atan}\left(\frac{S_{23}}{S_{33}}\right) * \beta_{max}^{Torsion}\right)\right\} + \\ &\left\{\left(\text{atan}\left(\frac{S_{22}}{S_{23}}\right) * \beta_{\text{max}}^{\text{Axial}} - \text{atan}\left(\frac{S_{23}}{S_{33}}\right) * \beta_{max}^{Torsion}\right)\right\} * \cos\left(\phi^{\text{Axial}} - \phi^{\text{Torsion}}\right)\end{aligned} \tag{10}$$

Table 5. Maximum values of the sensitivity analysis for P and NP and respective applied stress—results obtained by FEA.

Period for Maximum Values of the Sensitivity Analysis [0.125 s]				
NP Loading Path		**Applied Stress**	**P Loading Path**	
$\beta_{max}^{Tension}$	$\beta_{max}^{Torsion}$	**[MPa]**	$\beta_{max}^{Tension}$	$\beta_{max}^{Torsion}$
0	0	77	0	0
N/A	N/A	85	0.06262	0.02708
0.03992	0	95	N/A	N/A
N/A	N/A	100	N/A	N/A
0.03616	0	105	0.05063	0.02196
N/A	N/A	110	0.04909	0.02118

N/A: "not available".

Equation (10) is then used to estimate the opening angle of the notch crack for magnesium alloys, where S22 and S33 are the normal stresses in the yy and zz directions; both are perpendicular to the longitudinal direction of the specimen (xx direction). S23 is the shear stress in the yz direction. The notch is aligned with the yy direction. Here, S is used to represent the stresses instead of the traditional sigma or tau symbols. This is to indicate that these stresses are from FEA simulations and not from the traditional analytical expressions.

The values of $\beta_{\text{max}}^{axial}$ and $\beta_{\text{max}}^{torison}$ are the maximum values of the sensitivity analysis that result when the maximum axial load occurs. The value ϕ_{axial} and $\phi_{torison}$ corresponds to the angle of the load path for the period of 0 s, see Figure 2. The first ϕ, as described in

Equation (10), in this case ϕ_{axial}, is the angle associated with the axial load. The second ϕ, as described in Equation (10), in this case $\phi_{torison}$, is the angle associated with the torsion.

The sensitivity analysis is performed for the stress tensor shown in Equation (5). For this purpose, the determinant of Equation (5) (stress tensor) is calculated, and then the σ and τ stresses, Equations (6) and (9), are substituted into Equation (5). Then the derivative with respect to R (the radius of the sample) is performed.

3.3. Finite Element Analysis

A finite element analysis (FEA) is performed to obtain the developed stresses (i.e., the stresses after adapting the material to the type and intensity of loading) in order to determine the opening angle of the notch crack using expression 10. For this purpose, a specimen test was modulated in the ABAQUS® 2021 software according to the specifications of the E606/E606M-21 Standard Test Method for Strain-Controlled Fatigue Testing.

The indentation (notch) was placed in the negative direction of the XX axis, it has a cylindrical shape with a circular cross-section with a radius of 0.15 mm, and the notch is 30 mm long in the longitudinal direction, as shown in Figures 1 and 4b.

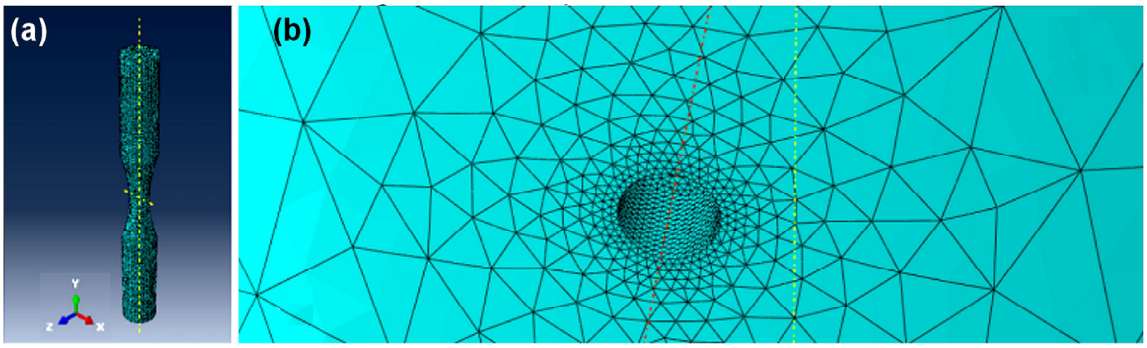

Figure 4. Computational image of the specimen: (**a**) specimen with mesh; and (**b**) notch, the yellow line represents the longitudinal axis and the red line the radial direction of the specimen).

The element used in the FEA was the parametric element "C30D10", a square tetrahedral element. The simulated sample in the FEA with notch has a mesh with 256,137 elements. The computational analysis of the sample with notch was performed using the Chaboche plasticity model, as described in Sections 2.2 and 2.3.

After creating the sample in the FEA model including the notch and after adding the Chaboche plasticity model, one end was bonded, and the loads shown in Figure 2 (axial and torsional loading) were applied to the other end cyclically by repeating the load blocks shown in Figure 2. The stresses developed were then determined in order to calculate the NCOA.

4. Results and Discussion

The sensitivity analysis, photos of the fracture surface and the crack initiation angle of the sample with the corresponding discussion are presented in the current section.

4.1. Sensitivity Analysis

Figure 5 shows the evolution of the β parameters (sensitive analysis) used in the proposed model to predict the fatigue crack orientation at the earliest stages of propagation. These results were obtained through simulations in FEA.

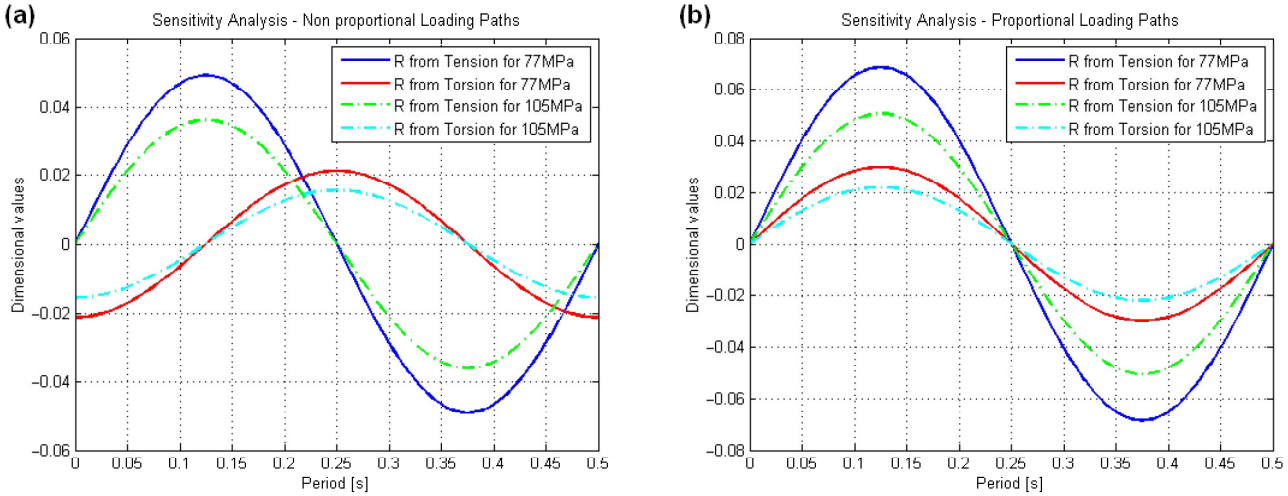

Figure 5. Sensitivity analysis: (**a**) NP loading path, and (**b**) P loading path.

It can also be seen that the maximum values of the sensitivity analysis occur for the time span of 0.125 s for both load paths. Different angles between the normal stresses and the shear stresses were then calculated and multiplied by the maximum sensitivity values, as shown in Equation (10). The normal and shear stresses assumed in Equation (10) are the maximum values near the notch and for the maximum values of the sensitivity analysis.

For pure tension of a cylindrical component, the crack angle is 0°. For pure torsion of a cylindrical component, the maximum crack angle is ±45°. Because both loading paths, proportional and non-proportional, as described in Figure 2, are a combination of tension and torsion, it is expected that NCOA ∈ [0°, ±45°]. Once the features of the loading path are different, it is expected that the NCOA will also be different. The notch crack opening angle was calculated using the following proposed stress-based analytical expression:

The maximum values of β for tension and torsion as a result of the sensitivity analysis, are shown in Table 5.

NP and P stand for non-proportional and proportional load paths, respectively. N/A stands for unavailable results, as there were no tests for this load. The values listed in Table 5 were used in the stress-based model to calculate the NCOA, as described in Equation (10). The maximum values of the stresses for maximum sensitivity occur near the notch and in the fourth quadrant. The β-values obtained from the sensitivity analysis are the maximum values as shown in this paper, presented in Table 5. The maximum values of β are obtained for the period of 0.125s and are specific to each load path.

4.2. Correlation between Experiments and NCOA Prediction

Figure 6 summarizes the experimental results for the crack initiation angle of magnesium alloy AZ31BF subjected to non-proportional and proportional load paths. In each subfigure of Figure 6, the NCOA estimated for the respective sample is shown in blue.

The summary of the maximum stresses near the notch during the FEA for the conditions described in this paper, as well as the summary of the NCOA and the stresses observed during the experiments in the laboratory and the respective errors obtained for both loading paths, are shown in Table 6. The positive signal and the negative signal of the stress represent compression and tension, respectively. All stresses are given in MPa.

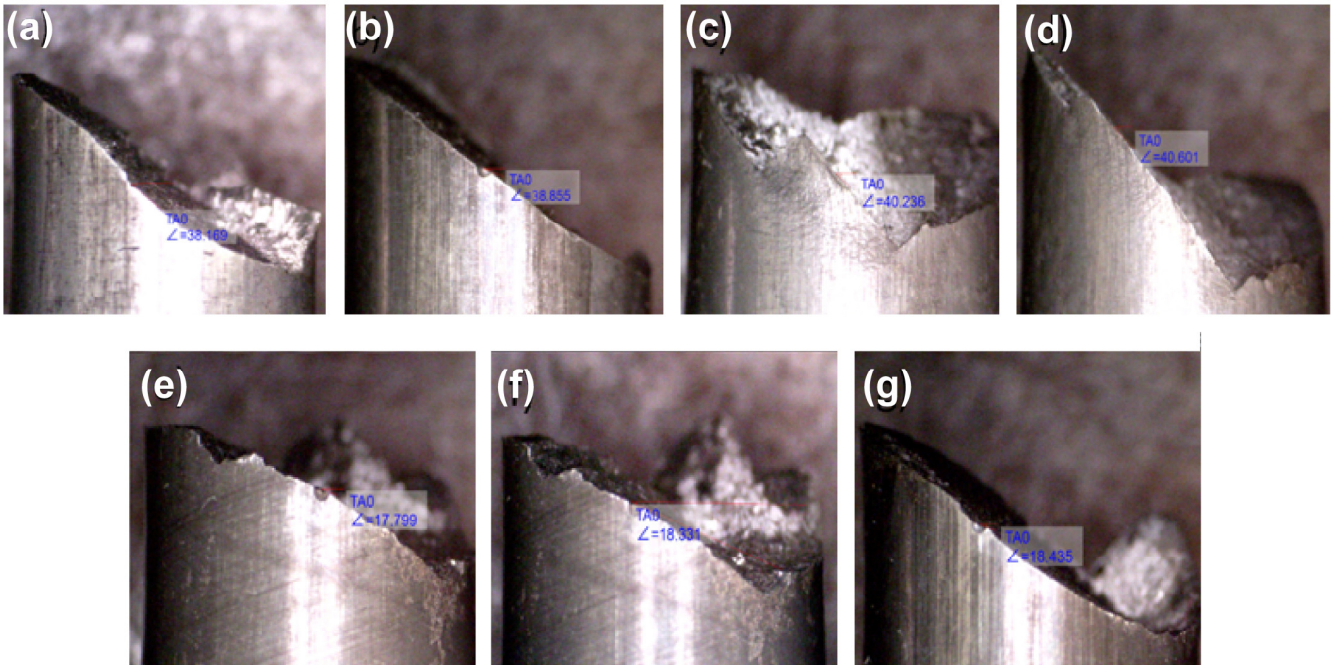

Figure 6. Photograph of the NCOA for: (**a**) 77MPa OP; (**b**) 85MPa OP; (**c**) 105MPa OP; (**d**) 110MPa OP; (**e**) 77MPa P; (**f**) 95MPa P and (**g**) 105MPa P.

Table 6. Summary of the stresses, the experimental angle, the calculated crack angle and the respective error.

Mises Stress [MPa]	Stress NP Loading Path			Stress P Loading Path			Non Proportional			Proportional		
	S22 [MPa]	S23 [MPa]	S33 [MPa]	S22 [MPa]	S23 [MPa]	S33 [MPa]	Exp. Angle	Crack Angle	Error [%]	Exp. Angle	Crack Angle	Error [%]
77	13.33	−3.76	2.51	46.0	−17.24	40.18	−18.05	−17.99	0.343	−38.16	−38.07	0.256
85	N/A	N/A	N/A	50.62	−18.97	44.2	N/A	N/A	N/A	−38.85	−38.79	0.162
95	16.45	−4.63	3.09	N/A	N/A	N/A	−18.79	−17.99	0.475	N/A	N/A	N/A
105	18.3	−5.13	3.42	62.39	−23.38	54.50	−18.13	−18.07	0.308	−40.23	−40.21	0.054
110	N/A	N/A	N/A	64.73	−24.25	56.51	N/A	N/A	N/A	−40.60	−40.40	0.49

N/A: "not available".

Based on the results, it was found that cracks appear on the surface of the sample. This is due to the fact that the shear stress at the surface is greater, resulting in a higher combined equivalent stress at the surface of the sample. This means that the cracks never occur within the notch, but at the interface between the surface and the notch. The NCOA occurred between [0°, ±45°] as expected. The exact values of NCOA calculated using the proposed analytical stress-based model, and those observed in the laboratory experiments are shown in Table 6.

The NCOA occurs in the XY plane. The FEA shows that the maximum value of the stresses occurs near the notch and in the fourth quadrant of the XY plane. However, the crack extends along the second and fourth quadrant of the XY plane, as you can see below.

Once the combination of axial and torsional loading was different in each loading path with the respective in-phase or out-of-phase angle, a different NCOA was expected. If you analyze Figure 7 in detail, you can see that the value of the sensitivity of each load, axial and torsional, is quite different in each load path. In the first half of the period range, [0 s; 0.250 s], the maximum value of sensitivity occurs, more precisely at 0.125 s. In the first half of the proportional load path, however, the sensitivity for the axial load is always higher than that for the torsion.

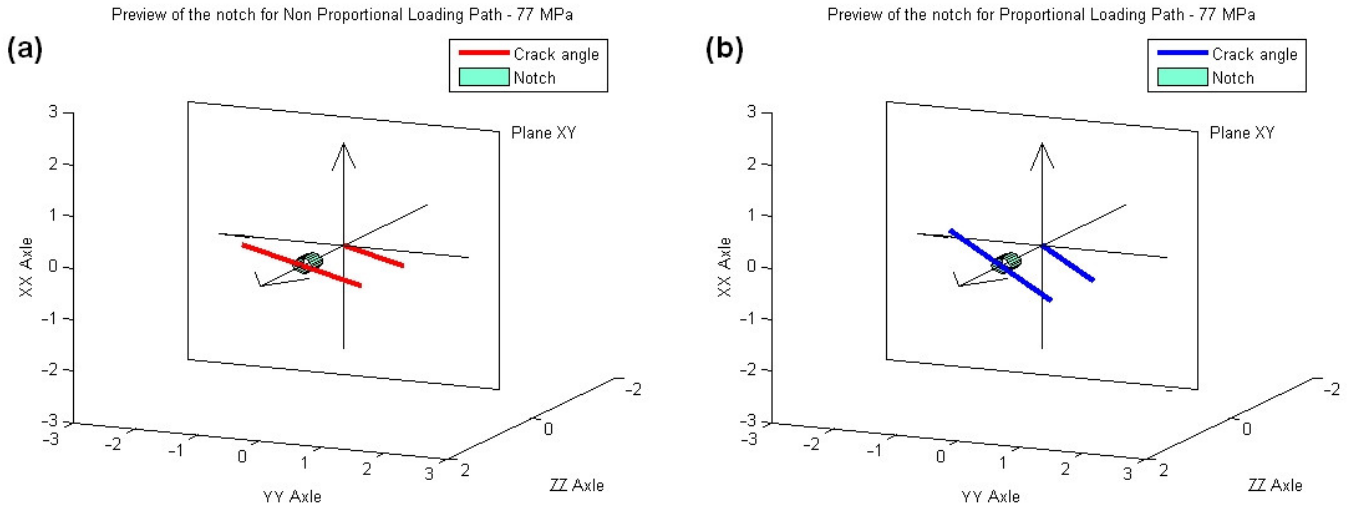

Figure 7. NCOA at the surface and in the plane XY: (**a**) NP loading path; (**b**) P loading path.

The same is not true for the non-proportional load path in the remaining period range. In a detailed analysis of the sensitivity analysis (see Figure 5), the sensitivity of the torsion is greater than that of the axial load, approximately in the second half of the period range. This is a direct consequence of the out-of-phase load path, which leads to a different NCOA.

5. Conclusions

The analytical model proposed to calculate the NCOA agrees with the experimental results. The error between the stress-based model and the results obtained in the tests is acceptable. In fact, the maximum error is below 0.5% in all the cases studied. The maximum values for the sensitivity analysis occur in the first half of the loading period range, i.e., at 0.125s for both stress paths. For the proportional load path, the sensitivity value is always higher than the torsion value due to the axial load. For the non-proportional load path, however, the sensitivity of the axial load is lower than the sensitivity of the torsion, but only in part of the period range. This is a consequence of the external phase shift angle, which has a direct influence on the NCOA. As expected, the NCOA occurred in the range [0°, ±45°]. In fact, it occurred at negative values in both cases. The NCOA was approximately 18° and 39° for the non-proportional and proportional load paths, respectively. The NCOA is a property of the load path and the respective in-phase or out-of-phase angle. In the experiments, it was found that the crack plane was the XY plane and the crack occurred on the surface of the specimen and along the second and fourth quadrants of the XY plane. The XY plane was perpendicular to the direction of the notch.

Author Contributions: Conceptualization, H.V. and L.R.; methodology, H.V.; software, H.V. and V.A.; validation, L.R. and V.A.; formal analysis, L.R.; investigation, V.A.; resources, L.R.; data curation, V.A. and L.R.; writing—original draft preparation, H.V.; writing—review and editing, L.R. and V.A.; visualization, V.A. and H.V.; supervision, L.R.; project administration, L.R.; funding acquisition, L.R. All authors have read and agreed to the published version of the manuscript.

Funding: This work was supported by FCT, through IDMEC, under LAETA, project UIDB/50022/2020.

Data Availability Statement: The original contributions presented in the study are included in the article, further inquiries can be directed to the corresponding authors.

Acknowledgments: The authors gratefully acknowledge the support from FCT–Fundação para a Ciência e Tecnologia (Portuguese Foundation for Science and Technology), through IDMEC, under LAETA, project UIDB/50022/2020.

Conflicts of Interest: The authors declare no conflicts of interest.

References

1. Collins, J.A. *Failure of Materials in Mechanical Design: Analysis, Prediction, Prevention*; John Wiley & Sons: Hoboken, NJ, USA, 1993.
2. Dieter, G.E.; Bacon, D. *Mechanical Metallurgy*; McGraw-Hill: New York, NY, USA, 1976; Volume 3.
3. Frost, N.E.; Marsh, K.J.; Pook, L.P. *Metal Fatigue*; Courier Corporation: North Chelmsford, MA, USA, 1999.
4. Faruq, N.Z.; Susmel, L. Proportional/Nonproportional Constant/Variable Amplitude Multiaxial Notch Fatigue: Cyclic Plasticity, Non-zero Mean Stresses, and Critical Distance/Plane. *Fatigue Fract. Eng. Mat. Struct.* **2019**, *42*, 1849–1873. [CrossRef]
5. Stephens, R.I.; Fatemi, A.; Stephens, R.R.; Fuchs, H.O. *Metal Fatigue in Engineering*; John Wiley & Sons: Hoboken, NJ, USA, 2000.
6. Neuber, H. *Theory of Notch Stresses: Principles for Exact Calculation of Strength with Reference to Structural Form and Material*; Clearinghouse for Federal Scientific and Technical Information: Springfield, OH, USA, 1961.
7. Peterson, R.E. Notch Sensitivity. In *Metal Fatigue*; McGraw-Hill: New York, NY, USA, 1959; pp. 293–306.
8. Gough, H.J. Engineering Steels under Combined Cyclic and Static Stresses. *Am. Soc. Mech. Eng.* **1950**, *160*, 417–440. [CrossRef]
9. Tipton, S.M.; Nelson, D.V. Advances in Multiaxial Fatigue Life Prediction for Components with Stress Concentrations. *Int. J. Fatigue* **1997**, *6*, 503–515.
10. Susmel, L.; Lazzarin, P. A Bi-parametric Wöhler Curve for High Cycle Multiaxial Fatigue Assessment. *Fatigue Fract. Eng. Mat. Struct.* **2002**, *25*, 63–78. [CrossRef]
11. Lazzarin, P.; Susmel, L. A Stress-based Method to Predict Lifetime under Multiaxial Fatigue Loadings. *Fatigue Fract. Eng. Mat. Struct.* **2003**, *26*, 1171–1187. [CrossRef]
12. Susmel, L. *Multiaxial Notch Fatigue*; Elsevier: Amsterdam, The Netherlands, 2009.
13. Taylor, D. The Theory of Critical Distances. *Eng. Fract. Mech.* **2008**, *75*, 1696–1705. [CrossRef]
14. Aghion, E.; Bronfin, B.; Eliezer, D. The Role of the Magnesium Industry in Protecting the Environment. *J. Mater. Process. Technol.* **2001**, *117*, 381–385. [CrossRef]
15. Blawert, C.; Hort, N.; Kainer, K.U. Automotive Applications of Magnesium and Its Alloys. *Trans. Indian. Inst. Met.* **2004**, *57*, 397–408.
16. Halsey, W.D.; Shores, L. *Collier's Encyclopedia*; Crowell-Collier Publishing: Springfield, OH, USA, 1965.
17. Polmear, I.J.; Polmear, I.J. *Light Alloys: Metallurgy of the Light Metals*, 3rd ed.; Metallurgy and Materials Science Series; Arnold: London, UK, 1999; ISBN 978-0-340-63207-9.
18. Mordike, B.L.; Ebert, T. Magnesium: Properties—Applications—Potential. *Mater. Sci. Eng. A* **2001**, *302*, 37–45. [CrossRef]
19. Oršulová, T.; Palček, P.; Uhríčik, M. Comparison of Temperature Dependence of Internal Damping of Selected Magnesium Alloys. *Prod. Eng. Arch.* **2019**, *22*, 7–10. [CrossRef]
20. Begum, S.; Chen, D.L.; Xu, S.; Luo, A.A. Low Cycle Fatigue Properties of an Extruded AZ31 Magnesium Alloy. *Int. J. Fatigue* **2009**, *31*, 726–735. [CrossRef]
21. Yang, F.; Yin, S.M.; Li, S.X.; Zhang, Z.F. Crack Initiation Mechanism of Extruded AZ31 Magnesium Alloy in the very High Cycle Fatigue Regime. *Mater. Sci. Eng. A* **2008**, *491*, 131–136. [CrossRef]
22. Mayer, H.; Papakyriacou, M.; Zettl, B.; Stanzl-Tschegg, S.E. Influence of Porosity on the Fatigue Limit of Die Cast Magnesium and Aluminium Alloys. *Int. J. Fatigue* **2003**, *25*, 245–256. [CrossRef]
23. Videira, H. Caracterização e Avaliação do Comportamento Mecânico da Liga de Magnésio AZ31B sob Fadiga Multiaxial na Presença de um Entalhe. Master's Thesis, Instituto Superior Técnico, Universidade de Lisboa, Lisboa, Portugal, 2013.
24. Bedoya Velásquez, S.; Restrepo Aguirre, A.S.; Femández-Morales, P.; Mendoza, E. Comparison by Computational Modeling of Mechanical Performance of Aeronautical Parts Made of Magnesium and Aluminum Alloys. *Prospectiva* **2017**, *15*, 26–32.
25. Anes, V.; Reis, L.; Freitas, M. Fatigue Damage Map of AZ31B-F Magnesium Alloys under Multiaxial Loading Conditions. *Metals* **2021**, *11*, 1616. [CrossRef]
26. Lee, H.W.; Basaran, C. A Review of Damage, Void Evolution, and Fatigue Life Prediction Models. *Metals* **2021**, *11*, 609. [CrossRef]
27. Anes, V.; Bumba, F.; Reis, L.; Freitas, M. Determination of the Relationship between Proportional and Non-Proportional Fatigue Damage in Magnesium Alloy AZ31 BF. *Crystals* **2023**, *13*, 688. [CrossRef]
28. Anes, V.; Moreira, R.; Reis, L.; Freitas, M. Simulation of the Cyclic Stress–Strain Behavior of the Magnesium Alloy AZ31B-F under Multiaxial Loading. *Crystals* **2023**, *13*, 969. [CrossRef]
29. Videira, H.; Anes, V.; Freitas, M.; Reis, L. Characterization and Evaluation of the Mechanical Behaviour of the Magnesium Alloy AZ31B in Multiaxial Fatigue in the Presence of a Notch. *Procedia Struct. Integr.* **2016**, *1*, 197–204. [CrossRef]
30. *ASTM E8*; E28 Committee Test Methods for Tension Testing of Metallic Materials. ASTM International: West Conshohocken, PA, USA, 2022.
31. *ASTM E606*; E08 Committee Test Method for Strain-Controlled Fatigue Testing. ASTM International: West Conshohocken, PA, USA, 2021.
32. Anes, V.; Reis, L.; Li, B.; Freitas, M. Crack Path Evaluation on HC and BCC Microstructures under Multiaxial Cyclic Loading. *Int. J. Fatigue* **2014**, *58*, 102–113. [CrossRef]
33. Yu, Q.; Zhang, J.; Jiang, Y.; Li, Q. Multiaxial Fatigue of Extruded AZ61A Magnesium Alloy. *Int. J. Fatigue* **2011**, *33*, 437–447. [CrossRef]
34. Zúberová, Z.; Kunz, L.; Lamark, T.T.; Estrin, Y.; Janeček, M. Fatigue and Tensile Behavior of Cast, Hot-Rolled, and Severely Plastically Deformed AZ31 Magnesium Alloy. *Metall. Mater. Trans. A* **2007**, *38*, 1934–1940. [CrossRef]

35. Lopez, Z.; Fatemi, A. A Method of Predicting Cyclic Stress–Strain Curve from Tensile Properties for Steels. *Mater. Sci. Eng. A* **2012**, *556*, 540–550. [CrossRef]
36. Knezevic, M.; Levinson, A.; Harris, R.; Mishra, R.K.; Doherty, R.D.; Kalidindi, S.R. Deformation Twinning in AZ31: Influence on Strain Hardening and Texture Evolution. *Acta Mater.* **2010**, *58*, 6230–6242. [CrossRef]
37. Polák, J.; Klesnil, M.; Lukáš, P. High Cycle Plastic Stress-Strain Response of Metals. *Mater. Sci. Eng.* **1974**, *15*, 231–237. [CrossRef]
38. Socie, D.; Marquis, G. *Multiaxial Fatigue*; Society of Automotive Engineers: Warrendale, PA, USA, 2000.
39. Fatemi, A.; Socie, D.F. A Critical Plane Approach to Multiaxial Fatigue Damage Including Out-of-Phase Loading. *Fatigue Fract. Eng. Mat. Struct.* **1988**, *11*, 149–165. [CrossRef]
40. Xia, Z.C.; Hutchinson, J.W. Crack Tip Fields in Strain Gradient Plasticity. *J. Mech. Phys. Solids* **1996**, *44*, 1621–1648. [CrossRef]
41. Li, H.; Chandra, N. Analysis of Crack Growth and Crack-Tip Plasticity in Ductile Materials Using Cohesive Zone Models. *Int. J. Plast.* **2003**, *19*, 849–882. [CrossRef]
42. Chen, W.-F.; Han, D.J. *Plasticity for Structural Engineers*; J. Ross Pub: Fort Lauderdale, FL, USA, 2007; ISBN 978-1-932159-75-2.
43. Chaboche, J.L. Constitutive Equations for Cyclic Plasticity and Cyclic Viscoplasticity. *Int. J. Plast.* **1989**, *5*, 247–302. [CrossRef]
44. Chaboche, J.L. A Review of Some Plasticity and Viscoplasticity Constitutive Theories. *Int. J. Plast.* **2008**, *24*, 1642–1693. [CrossRef]
45. Lemaître, J.; Chaboche, J.-L. *Mechanics of Solid Materials*; Cambridge University Press: Cambridge, UK, 1990; ISBN 978-0-521-32853-1.
46. Hibbitt, Karlsson & Sorensen, Inc. *Abaqus/CAE User's Manual*; Abaqus: Johnston, RI, USA, 2020.